Translational Oncology
www.transonc.com

Volume 6 Number 5 October 2013 pp. 562–572 562

The Effect of Molecular Weight, PK, and Valency on Tumor Biodistribution and Efficacy of Antibody-Based Drugs[1,2]

Ruth Muchekehu*, Dingguo Liu*, Mark Horn*, Lioudmila Campbell*, Joselyn Del Rosario*, Michael Bacica*, Haim Moskowitz*, Trina Osothprarop*, Anouk Dirksen*, Venkata Doppalapudi*, Allan Kaspar*, Steven R. Pirie-Shepherd† and Julia Coronella*

*CoxV Pfizer Worldwide Research and Development, San Diego, CA; †Pfizer Worldwide Research and Development, Oncology Research Unit, San Diego, CA

Abstract

Poor drug delivery and penetration of antibody-mediated therapies pose significant obstacles to effective treatment of solid tumors. This study explored the role of pharmacokinetics, valency, and molecular weight in maximizing drug delivery. Biodistribution of a fibroblast growth factor receptor 4 (FGFR4) targeting CovX-body (an FGFR4-binding peptide covalently linked to a nontargeting IgG scaffold; 150 kDa) and enzymatically generated FGFR4 targeting $F(ab)_2$ (100 kDa) and Fab (50 kDa) fragments was measured. Peak tumor levels were achieved in 1 to 2 hours for Fab and $F(ab)_2$ *versus* 8 hours for IgG, and the percentage injected dose in tumors was 0.45%, 0.5%, and 2.5%, respectively, compared to 0.3%, 2%, and 6% of their nontargeting controls. To explore the contribution of multivalent binding, homodimeric peptides were conjugated to the different sized scaffolds, creating FGFR4 targeting IgG and $F(ab)_2$ with four peptides and Fab with two peptides. Increased valency resulted in an increase in cell surface binding of the bivalent constructs. There was an inverse relationship between valency and intratumoral drug concentration, consistent with targeted consumption. Immunohistochemical analysis demonstrated increased size and increased cell binding decreased tumor penetration. The binding site barrier hypothesis suggests that limited tumor penetration, as a result of high-affinity binding, could result in decreased efficacy. In our studies, increased target binding translated into superior efficacy of the IgG instead, because of superior inhibition of FGFR4 proliferation pathways and dosing through the binding site barrier. Increasing valency is therefore an effective way to increase the efficacy of antibody-based drugs.

Translational Oncology (2013) 6, 562–572

Introduction

Effective antibody therapies for targeting solid tumors are limited by poor penetration [1] and very low percent of injected dose (ID) reaching tumor [2]. Limited tumor penetration, caused by heterogeneous antigen expression [3] and blood supply [4], increased interstitial fluid pressure [5,6], as well as a so-called "binding site barrier" caused by high-affinity binding [7,8] are thought to contribute to less effective therapy by leaving viable cells untargeted [6]. As a consequence, alternatives to full-length IgG drugs have been widely investigated as a means of improving penetration [9,10].

Using a fibroblast growth factor receptor 4 (FGFR4) targeting CovX-body (a nontargeting IgG, covalently linked to an FGFR4-targeting peptide; 150 kDa) and enzymatically generated FGFR4 targeting $F(ab)_2$ (100 kDa) and Fab (50 kDa), we addressed the role of size, pharmacokinetics (PK), and avidity in tumor uptake, penetration, and ultimately efficacy.

Net drug levels in the tumor are driven by the PK properties (influenced by the dose and rate of plasma clearance), diffusion rate

Address all correspondence to: Steven R. Pirie-Shepherd, PhD, Pfizer Worldwide Research and Development, Oncology Research Unit, 10777 Science Center Drive, San Diego, CA 92121. E-mail: steven.pirie-shepherd@pfizer.com

[1]The authors disclose no potential conflicts of interest.

[2]This article refers to supplementary materials, which are designated by Figures W1 to W4 and are available online at www.transonc.com.

Received 17 May 2013; Revised 8 July 2013; Accepted 9 July 2013

DOI 10.1593/tlo.13409

(determined by the size and properties of the biotherapeutic), binding affinity, and rate of consumption of the drug [3,11,12].

IgG drug scaffolds inherently have excellent PK properties compared to other protein therapeutics because of both their molecular weight and ability to bind to the neonatal FcRn receptor, which recycles molecules that bind to them back to the serum maintaining elevated levels. The limited and heterogeneous tumor penetration of IgGs, however, has led to the use of smaller IgG fragments such as Fabs, scFv′s, and diabodies [13–15], which can, in theory, diffuse more efficiently through tumors, translating into more favorable ID ratios at earlier time points [16]. The use of antibody fragments though must be balanced by the shorter serum half-lives of non–Fc-containing constructs and the potential for more rapid distribution to normal tissues.

As well as PK, increased valency may also drive tumor biodistribution and efficacy, although the role of valency in tumor retention has yielded sometimes conflicting data. Increasing the valency increased the tumor uptake of human epidermal growth factor receptor 2 (HER2) binding diabodies [13,17], while increasing the valency of HER2 binding DARPins, decreased tumor uptake [18]. In those studies, increased valency was achieved by doubling the molecular weight, and therefore, the role of increasing the size (and potentially decreasing clearance time) in tumor uptake and retention could not be distinguished from the role of increased valency. However, in other studies using divalent $(scFv')_2$ molecules with zero, one, and two binding sites (same molecular weight), three-fold greater tumor retention was achieved with the construct with two binding sites [19].

A CovX-body is a peptide antibody fusion generated by conjugating a peptide on an azetidinone linker to a nonbinding humanized IgG1 monoclonal aldolase antibody [20]. The CovX-body technology allows the increase in the number of targeting peptides on our scaffolds from two to four on the bivalent IgG and $F(ab)_2$ and from one to two on the Fab using homodimeric FGFR4-targeting peptides. Increasing the valency of the constructs allows for the measurement of the role of increased valency on tumor uptake and penetration without significantly altering the molecular weight of the targeting scaffolds. Increasing the valency of our constructs increased cell binding of the bivalent constructs. It did not significantly increase tumor levels and decreased the penetration of the scaffolds into the tumor after a single dose, presenting a so-called "binding site barrier." The binding site barrier is the phenomenon whereby high-affinity antibodies accumulate around the vasculature and fail to distribute evenly throughout the tumor [8]. This dynamic barrier can be overcome by increasing the dose of the antibody [7,21]. In a multi-dose efficacy study comparing the tumor growth inhibition (TGI) of the IgG homodimer peptide construct *versus* the IgG monomer peptide, superior efficacy is observed with the homodimer IgG.

This current study demonstrates that in a single dose study, PK is the most important driver of maximal tumor levels. While higher levels of Fab were seen in the tumor after an hour than the IgG and $F(ab)_2$, superior maximal tumor concentrations are achieved with the IgG constructs. Increasing the avidity of an IgG is an effective way to maximize the efficacy of our targeting scaffolds.

Materials and Methods

Generating F(ab)$_2$ and Fab Scaffolds

CVX-2000, a humanized IgG1κ antibody [22], was digested overnight at 37°C with immobilized papain (Thermo Scientific, Waltham, MA) to produce Fab or immobilized pepsin (Thermo Scientific) to produce $F(ab)_2$. Fab fragments were purified by size exclusion followed by binding and elution to Protein L to separate Fab fragments from Fc fragments. $F(ab)_2$ fragments were purified by size exclusion, followed by cation exchange. Final fractions were analyzed on a Bioanalyzer (2100) protein electrophoresis chip (Agilent Technologies, Santa Clara, CA; Figure W1).

CVX-2000, $F(ab)_2$, and Fab constructs were conjugated with a monomeric or homodimeric FGFR4-targeting peptide through an azetidinone linker on the peptide, which reacts specifically with a lysine in the Fab arm [23]. The original FGFR4-targeting peptide was discovered by phage display and synthesized as described previously [20]. Nontargeted controls of the scaffolds were conjugated with a nonbinding peptide.

Direct binding ELISA. High-binding half-well 96-well plates were coated overnight at 4°C with recombinant human FGFR4-Fc (R&D Systems, Minneapolis, MN) or CVX-2000 anti-idiotype antibody for total scaffold measurements. After washing and blocking, titrated compounds were then added to the plates and incubated at room temperature for 1 hour, followed by incubation with goat anti-human IgG-HRP (Jackson ImmunoResearch Laboratories, West Grove, PA) at room temperature for 1 hour. Tetramethylbenzidine substrate solution (KPL, Gaithersburg, MD) was added, and OD_{450} was measured. Half maximal effective concentration (EC_{50}) value was obtained from the dose-response curve from the experiment.

Competitive ELISA. High-binding half-well 96-well plates were coated with goat anti-human IgG-Fc (Bethyl Laboratories, Montgomery, TX) at 4°C overnight. After washing and blocking, plates were incubated with recombinant human FGFR4-Fc for 1 hour at room temperature. Plates were washed, and titrated compounds were added in the presence of 50 ng/ml recombinant human FGF19 (R&D Systems) and 1 μg/ml heparan sulfate (Seikagaku/Amsbio, Lake Forest, CA) and incubated for 2 hours at room temperature. The bound compounds were detected by biotinylated anti-FGF19 antibody (R&D Systems), followed by incubation with streptavidin-HRP (Fitzgerald Industries, Acton, MA). OD_{450} was measured.

Surface plasmon resonance binding analysis. Surface plasmon resonance (SPR) binding analyses of anti-FGFR4 compounds were performed on ProteOn XPR36 instrument (BioRad, Hercules, CA) at 25°C. For kinetic analysis, recombinant human FGFR4-Fc protein (R&D Systems) was immobilized on parallel surfaces of a GLM chip (BioRad) by amine coupling according to the manufacturer's protocol. Running buffer was phosphate-buffered saline (PBS) with 300 mM sodium chloride and 0.05% (vol/vol) Tween 20. FGFR4 immobilization level was 990 RU for Fab binding and 640 RU for $F(ab)_2$ and IgG binding. Compounds were tested for binding to FGFR4 starting at 200 nM at a flow rate of 50 μl/min. Association was monitored for 180 seconds, and dissociation was monitored for 600 seconds. Chip was regenerated with 0.85% (vol/vol) phosphoric acid in water. Data were double-referenced to blank chip surface and buffer injection and fitted to 1:1 binding model with local R_{max} using ProteOn Manager software (BioRad) to determine kinetic rate constants and K_D. Kinetic constants are averaged from three independent experiments.

For evaluation of monomer and homodimer peptide–conjugated compounds by capture of the compounds, anti-idiotype monoclonal antibody for CVX-2000 was immobilized across all surfaces of a

GLM chip (BioRad) to 10,000 RU. Running buffer was PBS with 0.01% (vol/vol) Tween 20; 50 nM Fab, 10 nM $F(ab)_2$, 10 nM IgG monomer and 80 nM Fab, 20 nM $F(ab)_2$, 20 nM IgG homodimer-conjugated constructs were captured with anti-idiotype CVX-2000 antibody. FGFR4-Fc (10 nM; R&D Systems) protein was tested for binding to anti-FGFR4 compounds captured on the chip. Data were double-referenced to chip surface and buffer blank.

Huh-7 cell line. Huh-7 cells were obtained from Japan Health Science Research Resources Bank (Osaka, Japan; Cat. JCRB0403) and were in Dulbecco's modified Eagle's medium (Invitrogen, Carlsbad, CA) containing 10% FBS and maintained at 37°C and 5% CO_2.

Flow cytometry (FACS). Huh-7 cells were harvested with cell stripper and resuspended in FACS buffer (PBS + 10% FBS + 1% sodium azide). Cells were incubated with FGFR4-targeting scaffolds for 1 hour on ice. Cells were then washed and incubated with phycoerythrin (PE)-labeled Goat Anti-Human IgG, $F(ab')_2$ Fragment Specific secondary antibody (Jackson ImmunoResearch Laboratories) for 30 minutes. Cell binding was measured using a flow cytometer (BD Biosciences, San Diego, CA). Data were analyzed using FloJo software (TreeStar Inc, Ashland, OR).

PK in rodents. PK properties of constructs were assessed in 5-week-old male Swiss Webster mice weighing 18 to 20 g (Charles River Laboratories, Wilmington, MA). Compounds were administered intravenously (i.v.) at 10 mg/kg (n = 3), and blood samples were collected over a period of 5 days. Serum samples were prepared and analyzed for FGFR4 binding activity in binding ELISAs as described previously. Total scaffold levels were measured by binding to a CVX-2000 anti-idiotype antibody capture ELISA. Data were analyzed using WinNonlin software (Pharsight, St Louis, MO) to generate PK parameter estimates.

Preparation of near-infrared–conjugated constructs. FGFR4 targeting CovX-bodies (IgG) and $F(ab)_2$ and Fab constructs were labeled with IRDye 800CW (LI-COR Biosciences, Lincoln, NE). In brief, constructs were buffer exchanged into 50 mM sodium phosphate buffer (pH 7) and incubated with two equivalents of the dye to the antibody solution overnight at room temperature in the dark. Constructs were buffer exchanged several times in Amicon spin filters [50 kDa molecular weight cut off (MWCO)] to remove free dye. Dye-to-protein ratios were calculated according to the manufacturer's instructions using the A_{780} and A_{280} measurements.

In vivo *xenograft studies.* Xenografts were induced by subcutaneous implantation of Huh-7 tumor cells into 5- to 7-week-old female nu/nu mice (18-20 g at start of experiment) and allowed to grow to a volume of 200 to 400 mm^3 before initiation of treatment. Once tumors were established, mice were randomized to treatment groups on the basis of their tumor volumes for all *in vivo* studies described below.

In vivo *animal imaging.* Near-infrared–conjugated compounds were administered at 3 and 10 mg/kg by intraperitoneal (i.p.) injection (no significant difference in tumor uptake was observed in a pilot study comparing i.p. *vs* i.v. injection). Mice were anesthetized with 5% isoflurane for induction and maintained at 2% during image capture. The images were acquired at the indicated time points with an IVIS Lumina II Imaging System (PerkinElmer, Waltham, MA). A charge-coupled device (CCD) camera was used to collect the images. The images were analyzed using Living Image Software 4.0 (PerkinElmer). Regions of interest were quantified for mean pixel values.

Biodistribution studies. Mice were dosed at 30 mg/kg i.p. injection, and tumors were harvested at maximal accumulation time points derived from imaging study (1 hour for Fab, 2 hours for $F(ab)_2$, and 8 hours for IgG). Tumors and normal tissue were harvested for biodistribution and histologic evaluation. For total scaffold accumulation, tissues were homogenized using FastPrep Lysing Matrix D Tubes (MP Biomedicals, Santa Ana, CA). Tissues were placed in tubes in a cell lysis buffer (Cell Signaling Technology, Danvers, MA) containing HALT protease and phosphatase inhibitor cocktail (Thermo Scientific). Tubes were then pulse homogenized using a FastPrep-24 instrument (MP Biomedicals) followed by incubation on a shaker at 4°C for an hour. Samples were then spun at 14,000 rpm for 10 minutes, and the supernatant was removed to a fresh tube. Samples were then applied directly to CVX-2000 anti-idiotype capture binding ELISA plates for total scaffold measurement.

In vivo *efficacy study.* Mice were randomized into groups of 10 mice per group. All compounds were administered once weekly at 30 mg/kg by i.p. injection. Tumor volumes were measured once or twice weekly using calipers. Once the mean tumor volume of each treatment group exceeded 2000 mm^3, mice were killed by CO_2 asphyxiation followed by cervical dislocation. Tumors and normal tissue were harvested for histologic evaluation.

Immunohistochemistry

Tumors from the biodistribution study described above were fixed in formalin for 24 hours. Tumors were embedded in paraffin blocks, sectioned, and mounted for immunohistochemistry. After deparaffinization and rehydration, heat-mediated antigen retrieval was performed using antigen retrieval buffer (Abcam, Cambridge, United Kingdom) for 30 minutes. Slides were incubated in 1% H_2O_2 for 10 minutes followed by a blocking step for 30 minutes and primary antibody incubation. Blood vessels were detected using rabbit anti-CD31 antibody (Abcam; ab28364) overnight at 4°C. Sections were washed with PBS containing 0.01% Tween-20 and incubated with biotin anti-rabbit antibody (Jackson ImmunoResearch Laboratories) for 1 hour at room temperature followed by alkaline phosphatase–conjugated streptavidin (Jackson ImmunoResearch Laboratories) for 1 hour. Sections were washed and incubated with Vector Red Alkaline Phosphatase Substrate Kit (Vector Labs, Burlingame, CA) for 20 minutes. For dual staining, sections were washed and incubated in HRP-conjugated donkey anti-human IgG secondary antibody (Jackson ImmunoResearch Laboratories) overnight at 4°C. Sections were washed and incubated in DAB peroxidase substrate kit (Vector Labs), dehydrated, and mounted. Images were captured using a Leica SCN400 slide scanner (Leica Biosystems, Wetzlar, Germany) at ×40, and images were analyzed on Leica SCN400 Image Viewer software. Tumor penetration was quantified using Image-Pro plus software (Media Cybernetics Inc, Rockville, MD). Five isolated vessels were randomly selected per slide with the distance (in μm) the scaffolds penetrated measured twice with each measurement taken on opposite sides. Statistical significance was determined using Prism (GraphPad Software, San Diego, CA). FGFR4 staining was measured using a rat anti–hFGF-R4 primary antibody (R&D Systems), followed by an HRP-goat anti-rat IgG secondary antibody (Jackson ImmunoResearch

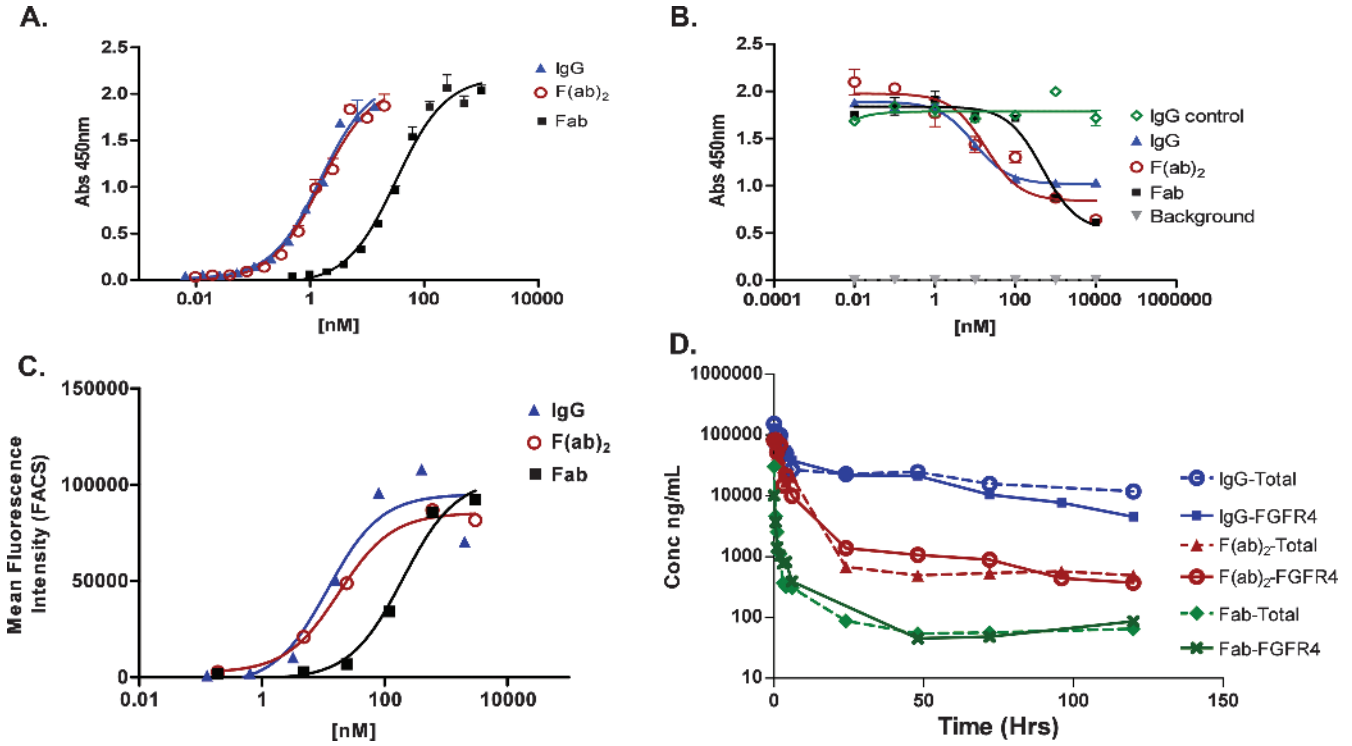

Figure 1. Characterization of FGFR4 binding scaffolds. (A) IgG, $F(ab)_2$, and Fab constructs bind specifically to FGFR4. (B) In an FGF19 competition ELISA, all constructs compete with FGF19 to bind to FGFR4. (C) All constructs bind to Huh-7 cells. (D) PK curves of IgG, $F(ab)_2$, and Fab following a single i.v. dose of 10 mg/kg in Swiss Webster mice. Both total and FGFR4 binding were measured as described in the Materials and Methods section.

Laboratories) for 1 hour at room temperature. Sections were washed and incubated using a DAB peroxidase substrate kit (Vector Labs).

Phospho-p44 Mitogen-Activated Protein Kinase (Extracellular Signal-Regulated Protein Kinase) Assay

Phospho-extracellular signal-regulated protein kinase (Erk1/2) was measured using a PathScan Phospho-p44 mitogen-activated protein kinase (MAPK) Sandwich ELISA Kit (Cell Signaling Technology; Cat. No. 7315). Homogenized tumor lysates from our biodistribution study were used according to the manufacturer's instructions. In brief, 100 µl was placed in microwells and incubated for 2 hours at 37°C. Wells were then washed four times with provided wash buffer and incubated with detection antibody for 1 hour at 37°C. Wells were washed and incubated in HRP-conjugated secondary antibody for 30 minutes at 37°C. Wells were washed and incubated with tetramethylbenzidine substrate for 10 minutes at 37°C, STOP solution was added, and OD_{450} was measured.

Internalization Studies

All scaffolds were biotinylated using EZ-Link Sulfo-NHS-LC-Biotin (Thermo Scientific) according to the manufacturer's instructions. Huh-7 cells were harvested using Cellstripper (Cellgro, Manassas, VA) and seeded at 100,000 cells per well in PBS4 (1 mM MgCl, 1 mM $CaCl_2$, 0.2% BSA, 5 mM glucose, and 10% FBS). Compounds were added and cell incubated at 37°C for 0, 15, 30, 60, and 120 minutes. Plates were placed on ice for 5 minutes to stop internalization and washed three times in PBS4. Cells were then incubated in Avidin (Sigma, St Louis, MO; at 100 µg/ml) at 4°C for 1 hour. Biocytin (Sigma; 1 mg/ml) was then added for 10 minutes. Cells were centrifuged, the supernatant was discarded, and cells were solubilized for 30 minutes at 4°C. Total amount of internalized scaffold was measured in supernatant by CVX-2000 anti-idiotype capture binding ELISA followed by incubation with streptavidin-HRP (Fitzgerald Industries).

Statistical Analyses

Data were analyzed either by two-way analysis of variance (ANOVA) with a Bonferroni post-test or by a two-tailed *t* test using Prism (GraphPad Software).

Results

In Vitro *Characterization of Scaffolds*

CVX-2000, $F(ab)_2$, and Fab constructs were conjugated with monomer FGFR4-targeting peptide as described in the Materials and Methods section.

Binding to FGFR4 was measured by ELISA and SPR. The IgG and $F(ab)_2$ constructs bind with an apparent binding affinity of

Table 1. Binding Affinity of IgG, $F(ab)_2$, and Fab Determined by SPR.

	k_{on} (M^{-1} s^{-1})	k_{off} (s^{-1})	K_D (nM)
Fab monomer	1.1×10^6	9.7×10^{-3}	8.5
Fab homodimer	9.4×10^5	7.1×10^{-3}	7.6
$F(ab)_2$ monomer	1.2×10^6	2.9×10^{-3}	2.5
$F(ab)_2$ homodimer	1.3×10^6	2.9×10^{-3}	2.3
IgG monomer	1.4×10^6	2.4×10^{-3}	1.8
IgG homodimer	3.6×10^6	1.9×10^{-3}	0.53

FGFR4 capture to measure monovalent interactions.

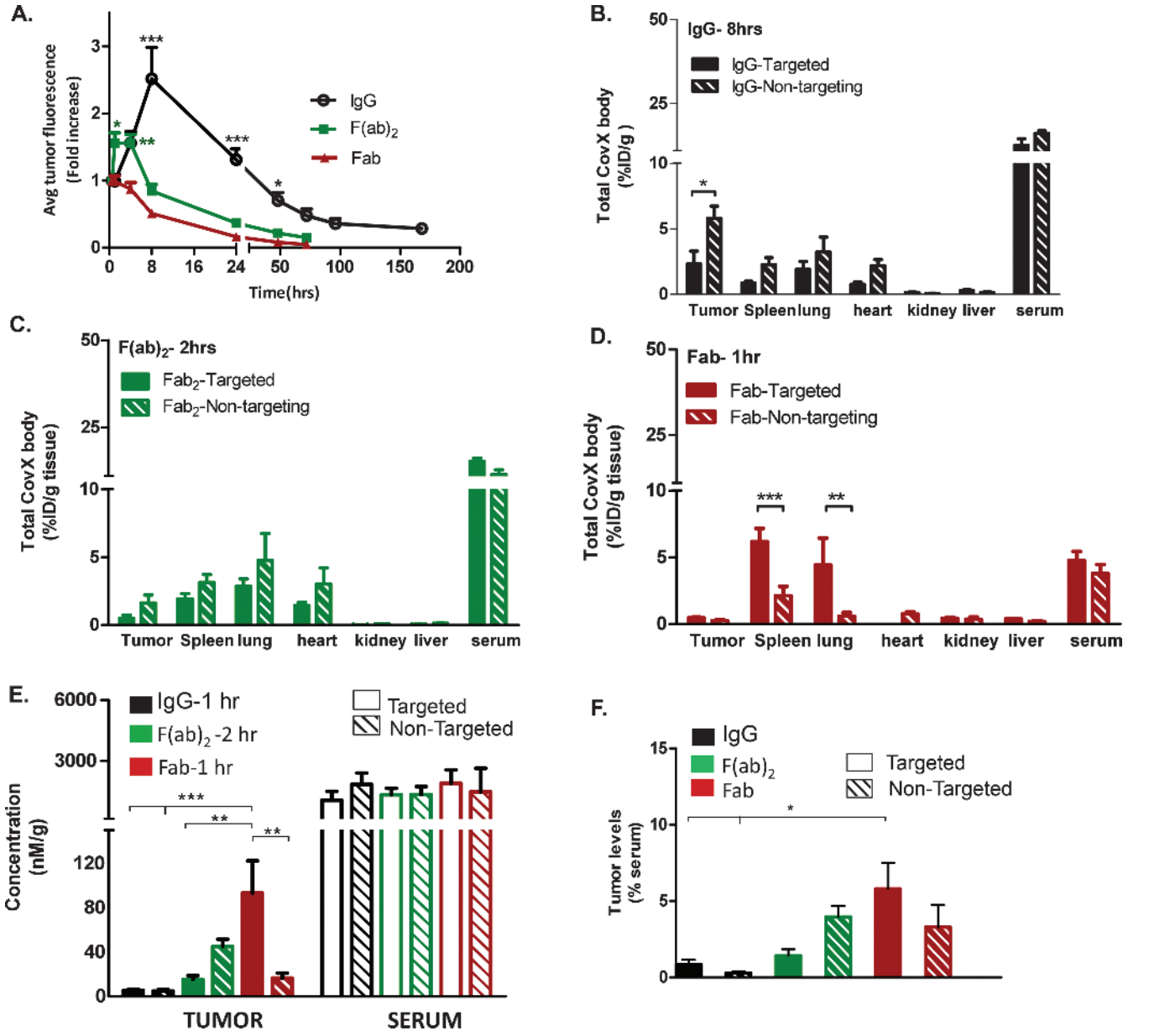

Figure 2. Biodistribution studies. (A) Time-dependent tumor uptake of IgG, $F(ab)_2$, and Fab. *In vivo* optical imaging of near infra-red (NIR)-conjugated constructs. Average signal intensities were quantified using regions of interest (ROIs) from the tumor sites. Data are presented as mean fold increase from initial image capture at 30 minutes ± SEM of eight mice (***$P < .001$, *$P < .05$; IgG *vs* both $F(ab)_2$ and Fab accumulation, *$P < .05$ and **$P < .01$; $F(ab)_2$ *vs* Fab accumulation by two-way ANOVA with Bonferroni post-test). Tumor and normal tissue uptake of (B) IgG 8 hours post dose (*$P < .05$), (C) $F(ab)_2$ 2 hours post dose, and (D) Fab 1 hour post dose (***$P < .001$, **$P < .01$ by two-way ANOVA with Bonferroni post-test). (E) IgG, $F(ab)_2$, and Fab tumor uptakes and serum levels compared at the early time points of 1 hour, 2 hours, and 1 hour, respectively. At this early time point with equivalent serum levels, the targeted Fab shows maximal accumulation levels compared to the $F(ab)_2$ and IgG (***$P < .001$, **$P < .01$ by one-way ANOVA with Bonferroni post-test). (F) Tumor to serum levels further demonstrate that the Fab construct accumulation is significantly higher than the IgG accumulation (*$P < .05$ by two-way ANOVA with Bonferroni post-test).

0.7 and 0.8 nM, respectively, whereas the Fab binds with a binding affinity of 11 nM (Figure 1*A* and Table 1). In a competition ELISA, the IgG and $F(ab)_2$ constructs compete for binding of FGF19 to FGFR4 with an half-maximal inhibitory concentration (IC_{50}) of 9 and 18 nM, respectively, whereas the Fab competes with an IC_{50} of 500 nM (Figure 1*B*).

Binding to Huh-7 cells, a hepatocellular carcinoma cell line that expresses high levels of FGFR4 [24], was measured by FACS. The IgG and $F(ab)_2$ constructs have a cell binding affinity of 9 and 18 nM, respectively, whereas the Fab has a binding affinity of 198 nM (Figure 1*C*).

Removal of the Fc and Reduction in Size Significantly Impact the PK Properties

PK studies were conducted by administering a single i.v. injection of 10 mg/kg of all compounds. The serum concentrations over time were measured using an FGFR4 and CVX-2000 anti-idiotype capture binding

ELISA for total scaffold measurements (Figure 1*D*). The intact FGFR4 targeting CovX-body has a β half-life in mice of 60 hours, compared to β half-lives of 4 to 6 and 1 to 3 hours for $F(ab)_2$ and Fab, respectively.

Time-Dependent Tumor Uptake

The constructs were labeled with a near-infrared dye IRDye 800CW to allow *in vivo* imaging of tumor penetration and retention in the Huh-7 hepatocellular carcinoma xenograft model. Compounds were administered at 3 mg/kg with a single i.p. injection, and tumor uptake was measured by image capture at the time points indicated (Figure 2*A*). Maximal accumulation of the IgG was seen after 8 hours (2.51 ± 0.47 fold increase in fluorescence relative to initial image captured at 30 minutes, $n = 8$; a representative image of IgG tumor uptake is shown in Figure W2), where accumulation was significantly higher than the Fab and $F(ab)_2$ constructs. The maximal accumulation for the $F(ab)_2$ construct was from 2 to 4 hours (1.63 ± 0.13 fold increase in fluorescence, $n = 8$), and at these time points, the $F(ab)_2$ accumulation was significantly higher than the Fab. Minimal accumulation of the Fab was observed after 1 hour in this imaging study (0.99 ± 0.08 fold increase in fluorescence, $n = 8$). In the more quantitative biodistribution study, where the tumors were homogenized and accumulation was measured by ELISA, accumulation of the Fab was observed after 1 hour (Figure 2*D*). This accumulation was also confirmed by immunohistochemistry (Figure 4*F*).

Tumor and Normal Tissue Uptake of Scaffolds

A biodistribution study was performed to determine the tumor and normal tissue uptake of the FGFR4-targeted constructs and their nontargeted controls. Animals were dosed at 30 mg/kg to quantify the tumor and normal tissue uptake. Tumor and normal tissue were harvested at the maximum accumulation time point derived from the previous imaging study: 8 hours post dose for the IgG (Figure 3*B*), 2 hours for the $F(ab)_2$ constructs (Figure 3*C*), and 1 hour for the Fab constructs (Figure 3*D*). Total scaffold accumulation was quantified by a CVX-2000 anti-idiotype capture binding ELISA. After 8 hours, accumulation of the nontargeted IgG is significantly higher than the targeted IgG (5.80 ± 0.92% *vs* 2.3 ± 0.99% ID, respectively; $P < .05$, $n = 5$). After 2 hours, there is a similar trend for the nontargeted $F(ab)_2$ *vs* targeted $F(ab)_2$ accumulation; however, this is not statistically significant (1.62 ± 0.58% *vs* 0.48 ± 0.24% ID, respectively; $P > .05$, $n = 5$). There was no significant difference between the targeted and nontargeted Fab after an hour (0.46 ± 0.07% *vs* 0.26 ± 0.06% ID, respectively; $P > .05$, $n = 5$). Both targeted and nontargeted constructs accumulate in tumors because of the enhanced permeability

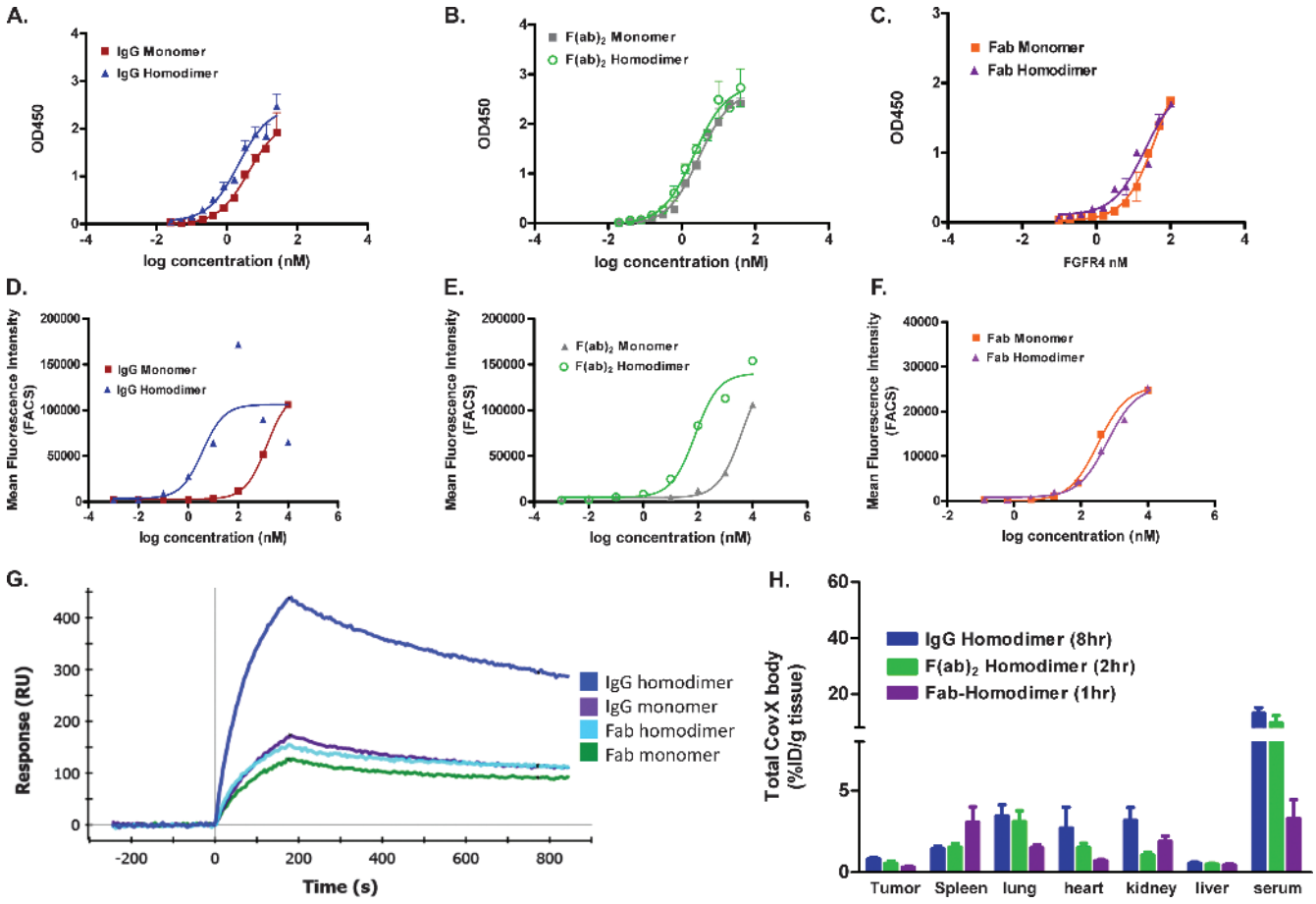

Figure 3. Increasing valency increases cell binding of bivalent constructs. (A–C) Monomer and homodimer peptide–conjugated constructs bind recombinant FGFR4 in a similar manner on an FGFR4 binding ELISA. Huh-7 cell binding of IgG (D) and $F(ab)_2$ (E) homodimer-conjugated constructs demonstrates a boost in cell binding affinity, whereas the Fab monomer and homodimer (F) have similar cell binding affinities. (G) Anti-idiotype capture levels of anti-FGFR4 monomer and homodimer compounds to measure multivalent interactions. Increased levels of FGFR4 binding is seen with the IgG homodimer. (H) Tumor and normal tissue uptake of homodimer peptide–conjugated IgG, $F(ab)_2$, and Fab (*$P < .05$ *vs* monomer IgG).

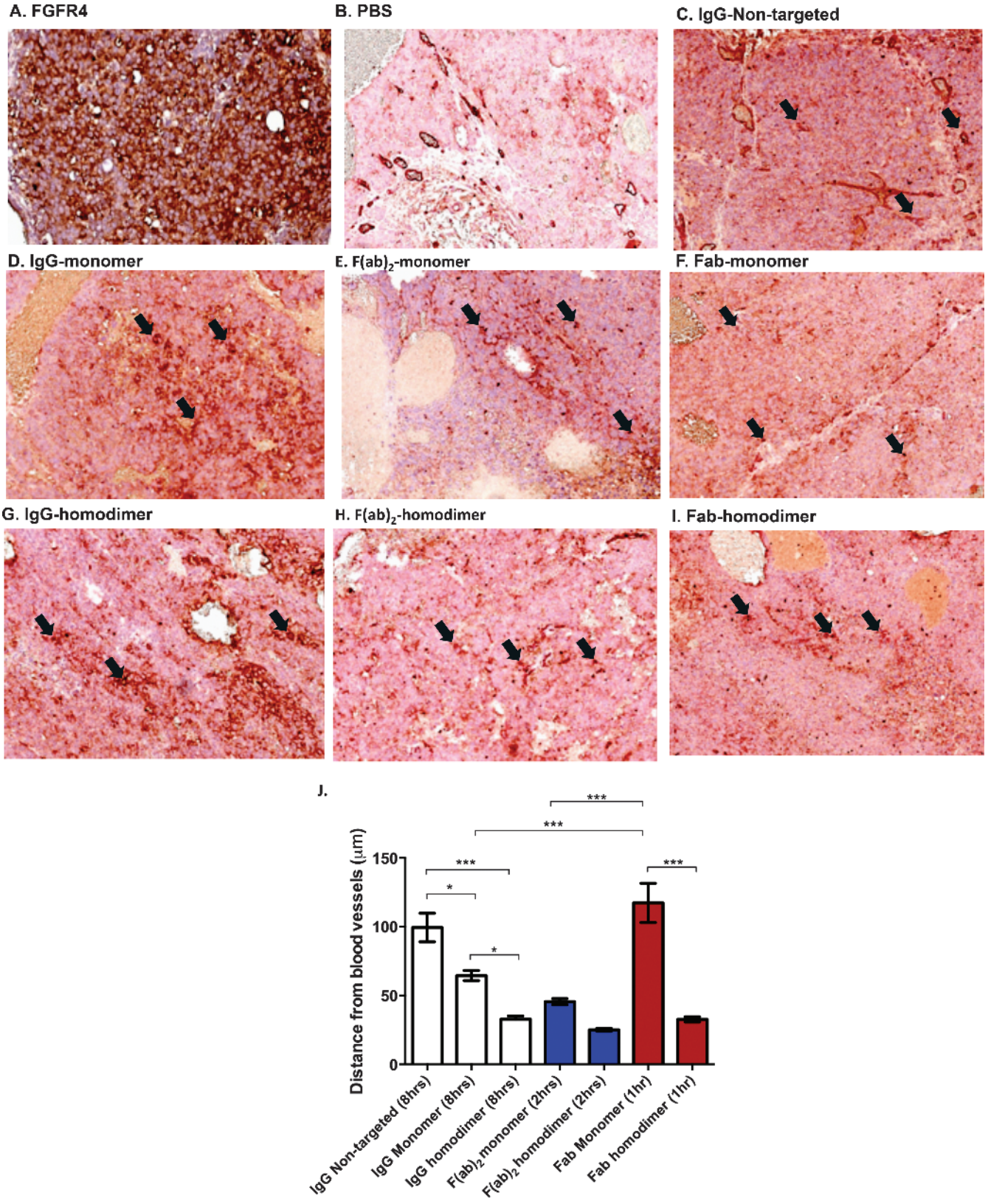

Figure 4. Increased avidity decreases penetration of scaffolds into the tumor. (A) FGFR4 staining in an adjacent section is shown. Dual staining for blood vessels (brick red) and human IgG (brown) is shown in (B) PBS-dosed animals, (C) nontargeted IgG (8 hours), monomer peptide–conjugated (D) IgG (8 hours), (E) $F(ab)_2$ (2 hours), (F) Fab (1 hour) and homodimer peptide–conjugated (G) IgG (8 hours), (H) $F(ab)_2$ (2 hours) and (I) Fab (1 hour). Arrows indicate blood vessels (red). Perivascular or diffuse construct staining from those points can be seen. (J) Plot of average distance from randomly selected blood vessels (mean ± SEM; $*P < .05$, $***P < .001$ by one-way ANOVA with Bonferroni post-test).

and retention effect; however, the differences in levels of the nontargeted *versus* targeted IgG and $F(ab)_2$ constructs may be due to internalization and "consumption" of the targeted constructs as shown in previous studies [25].

High levels of the targeted Fab accumulated in both the lung and spleen (4.42 ± 2.03% and 6.20 ± 1.00% ID, respectively; Figure 2*D*). Both the lung and spleen normally express FGFR4 [26,27], and the accumulation of the targeted Fab suggests that the FGFR4 binding peptide binds both human and mouse FGFR4. It also demonstrates the ability of the smaller Fab to rapidly accumulate in normal tissue.

Tumors were also harvested after 1 hour post dose with the IgG for an early time point comparison with the Fab and $F(ab)_2$ constructs (Figure W3). At this early time point, serum levels of the three constructs were comparable, allowing a comparison of tumor levels (Figure 2*E*). Tumor levels as a percent of serum show that the targeted Fab and nontargeted Fab constructs (5.81 ± 1.51% and 3.30 ± 1.29% serum, respectively) accumulate at a higher level than the targeted and nontargeted IgG (0.86 ± 0.27% and 0.28 ± 0.08% serum, respectively) and targeted $F(ab)_2$ constructs (1.43 ± 0.42% serum), whereas the nontargeted $F(ab)_2$ accumulation was not significantly different at this early time point (3.95 ± 1.29% serum; $P > .05$, $n = 5$; Figure 2*F*).

The Role of Increased Valency in Tumor Targeting

Increasing the number of targeting peptides from two to four on the IgG and $F(ab)_2$ constructs and from one to two on the Fab did not increase the apparent binding affinity to recombinant FGFR4 in an FGFR4 capture binding ELISA (Figure 3, *A*–*C*) or SPR (K_D = 0.5, 2.3, and 7.6 nM, respectively; Table 1). It did however increase the binding of the bivalent constructs to Huh-7 cells by 2 logs (Figure 3, *D* and *E*) but not of the Fab (Figure 3*F*).

In an SPR assay where the compounds (10 nM) were captured on the binding surface by the anti-idiotype CVX-2000 antibody, increased levels of FGFR4 binding could be measured on the tetravalent constructs, IgG (Figure 3*G*) and $F(ab)_2$ (data not shown) homodimer-conjugated constructs. These bind twice the amount of FGFR4 as the rest of the compounds, as would be expected as they each display four peptides. Comparable levels of monomer and homodimer constructs were captured with anti-idiotype CVX-2000 (Figure W4). This correlates with the increased cell binding we see with these constructs in the FACS assay (Figure 3, *D* and *E*).

Tumor and normal tissue accumulation of the homodimer-conjugated peptides showed that increasing the valency of the IgG, $F(ab)_2$, and Fab did not increase the tumor levels *versus* their monomer peptide–conjugated constructs (homodimer tumor accumulation of 0.82 ± 0.08%, 0.55 ± 0.12%, and 0.32 ± 0.06% ID, respectively, $n = 5$; Figure 3*G*).

The Role of Size and Valency in Tumor Penetration

High and evenly distributed levels of FGFR4 are seen in Huh-7 tumors (Figure 4*A*). Adjacent FGFR4 staining of all harvested tumors shown in Figure 4 all showed a similar high even distribution of FGFR4. A representative section in penetration of the nontargeted IgG construct in the tumor appears to be nonrestricted, and homogenous antibody staining is seen throughout the tumor (99.4 ± 10.4 μm penetration; Figure 4*C*).

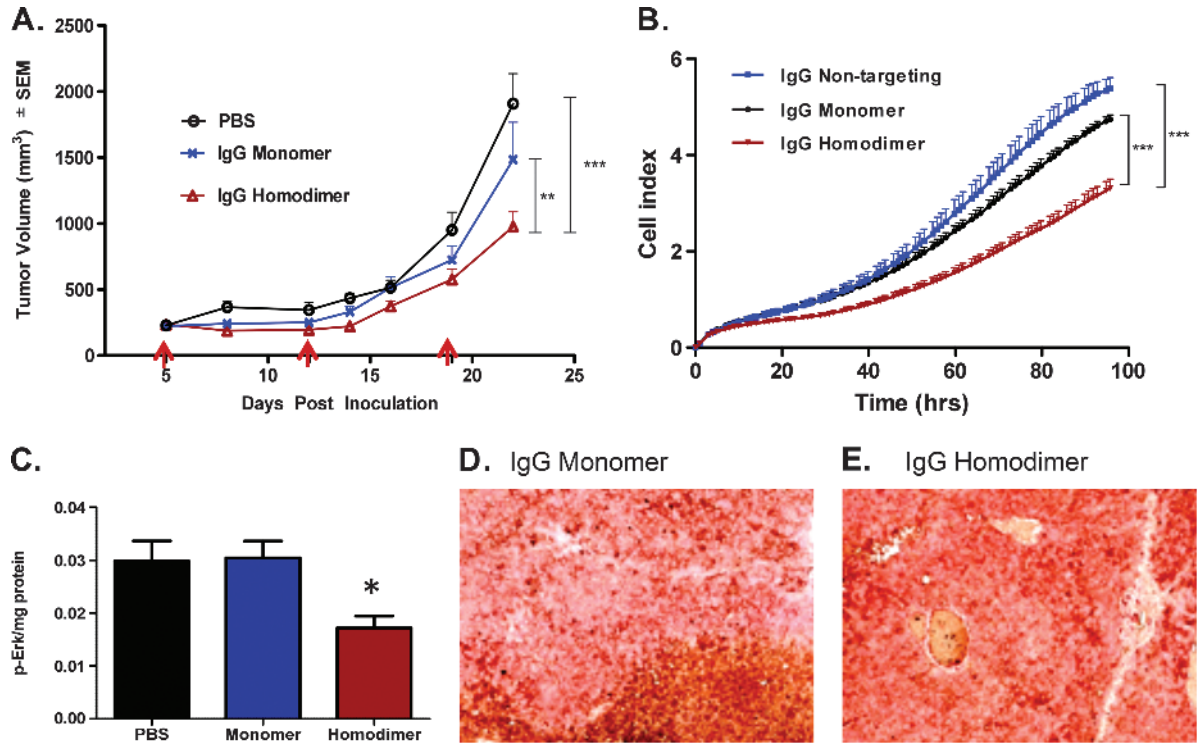

Figure 5. Increased avidity leads to superior efficacy. (A) *In vivo* xenograft study (i.p. dosing, 30 mg/kg once weekly) and (B) *in vitro* cell proliferation assay (12 nM compounds present in media for whole experiment). *$P < .05$, ***$P < .001$ by two-way ANOVA with Bonferroni post-test. Arrows indicate dosing. (C) Phospho-Erk levels measured in tumors harvested at the end of the efficacy study; *$P < .05$ *versus* PBS-dosed tumors by two-tailed Student's *t* test. Dual staining of blood vessels and human IgG of the tumors at the end of the efficacy study; (D) monomer peptide IgG dosed and (E) homodimer peptide IgG dosed.

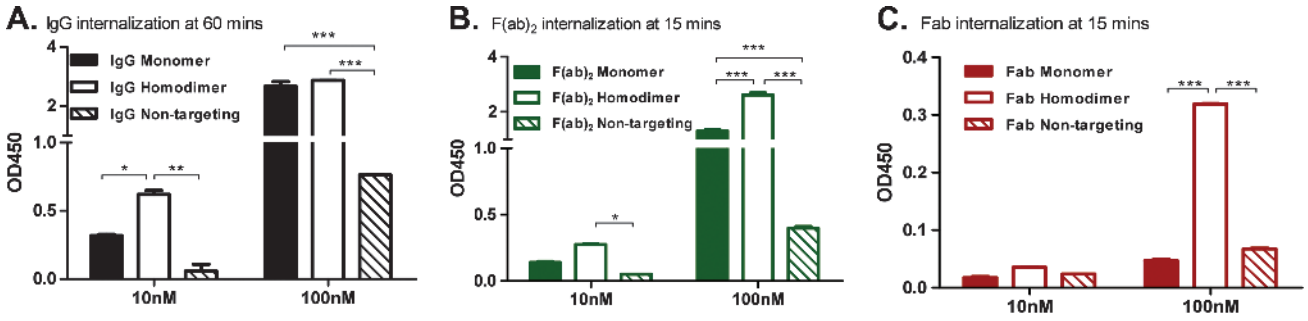

Figure 6. Multivalent binding is required for internalization. Internalization assays were conducted by incubating Huh-7 cells with biotinylated constructs at concentrations indicated at 37°C. Maximal internalization was seen at (A) 60 minutes for IgG constructs and 15 minutes for the (B) $F(ab)_2$ and (C) Fab constructs. The average ± SD is shown (*$P < .05$, **$P < .01$, ***$P < .001$ by two-way ANOVA with Bonferroni posttest).

However with the monomer peptide–conjugated IgG (Figure 4*D*) and $F(ab)_2$ (Figure 4*E*) constructs restricted, perivascular penetration is seen (64 ± 3.6 and 45.5 ± 2.3 μm, respectively).

More diffuse and even penetration is seen with the Fab monomer construct, demonstrating that the smaller scaffold is able to penetrate further and more evenly into the tumor (117.3 ± 14.3 μm; Figure 4*F*).

Increasing the affinity has been shown to decrease the penetration into the tumor from the vessels [25], due to the hypothetical "binding site barrier" phenomenon. Decreased tumor penetration is observed for the homodimeric peptide versions of the IgG, $F(ab)_2$, and Fab (32.7 ± 1.9, 25.1 ± 1.1, and 32.7 ± 1.9 μm, respectively; Figure 4, *G–I*).

Increasing Valency Leads to Superior Efficacy

The binding site barrier hypothesis predicts an inverse relationship between affinity and penetration, and this may subsequently translate into decreased efficacy. To determine if our observation of reduced penetration in our single dose study translates into reduced efficacy, we compared the TGI efficacy of the tetravalent (homodimer peptide conjugated) *versus* the bivalent (monomer peptide conjugated) IgG. We observed a superior TGI with the homodimer-conjugated IgG of 50% TGI *versus* 22% TGI with the monomer-conjugated IgG (975.4 ± 111.7 *vs* 1483 ± 266.5 mm^3, respectively; $P < .01$, $n = 10$; Figure 5*A*).

The increased TGI is likely due to several factors. In an *in vitro* proliferation assay, we observe superior inhibition of Huh-7 proliferation with the tetravalent construct compared to the monomer peptide–conjugated IgG (cell index of 3.3 ± 0.2 *vs* 5.4 ± 0.2, respectively, at end of the experiment; $P < .001$, $n = 3$; Figure 5*B*). Superior inhibition of the Erk1/2 signaling pathway was seen in tumors treated with the homodimer IgG *versus* monomer-conjugated IgG (0.017 ± 0.001 *vs* 0.030 ± 0.003, respectively; $P < .05$, $n = 5$; Figure 5*C*). Increasing the dose or concentration of a drug has been shown to overcome the binding site barrier [7]. We show in our multi-dosed tumors that we can overcome the "binding site barrier" observed in a single dose study and saturated levels of the IgG constructs are observed in sections of these tumors (Figure 5, *D* and *E*).

The Role of Targeting and Internalization on Net Drug Levels

In our tumor and normal tissue biodistribution study (Figure 2), it is clear that targeting is not necessary for tumor localization (targeting is, however, necessary for efficacy). In our study, we observed higher levels of the nontargeted IgG and $F(ab)_2$ in the tumor (Figure 2, *B* and *C*). To determine whether this is due to target-mediated internalization, *in vitro* internalization of our constructs conjugated to biotin was measured in Huh-7 cells as described in the Materials and Methods section. Robust internalization of the monomer and homodimer peptide IgG and $F(ab)_2$ was observed at 10 and 100 nM concentrations peaking at 60 minutes for the IgG (0.32 ± 0.01 and 2.67 ± 0.23 for the monomer and 0.62 ± 0.04 and 2.87 ± 0.002 for the homodimer, respectively; Figure 6*A*) and 15 minutes for the $F(ab)_2$ (0.14 ± 0.01 and 1.31 ± 0.05 for the monomer and 0.28 ± 0.004 and 2.61 ± 0.11 for the homodimer, respectively; Figure 6*B*). Negligible internalization was seen with the Fab constructs at 10 nM, whereas a significant increase in internalization of the homodimer-conjugated Fab *versus* the monomer Fab was seen at 100 nM (0.32 ± 0.001 *vs* 0.05 ± 0.003 respectively; Figure 6*C*).

Internalization and subsequent degradation of the IgG and $F(ab)_2$ constructs *in vivo* may contribute to the lower levels of the targeted constructs measured.

Discussion

The Role of Molecular Weight

Low accumulation levels of the $F(ab)_2$ and Fab constructs are achieved in a single dose study (Figure 2). At the early time points of 1 to 2 hours though, we can see that more of the Fab and $F(ab)_2$ constructs get into the tumor than the IgG (Figure 2, *E* and *F*).

Further, the Fab appears to rapidly and evenly distribute in the tumor (Figure 4*F*), demonstrating some benefit of reduced size. However, the Fab also ultimately produced lower maximum drug delivery than the IgG and a less favorable tumor/normal tissue ratio, reflecting less restricted diffusion into normal tissues as well (Figure 2*D*).

Although there have been some studies demonstrating improved tumor uptake and penetration with $F(ab)_2$ antibody scaffolds [28,29], the $F(ab)_2$ construct used in this study overall has the least favorable profile in terms of low accumulation (Figure 2*C*) and minimal tumor penetration (Figure 4*E*). The limited tumor penetration of the $F(ab)_2$ fragment in this current study may be due to internalization of our targeted construct (Figure 6*B*). Internalization and consumption of constructs may lead to decreased tumor penetration [25] and may contribute to the differences in the levels of tumor penetration seen in this current study and previously published work. The $F(ab)_2$ construct also resides in what is termed a "death valley" of

maximum tumor uptake *versus* size [30], too large to rapidly extravasate into the tumor tissue and too small to escape renal clearance.

Targeting Is Not Necessary for Tumor Localization

Both targeting and nontargeting versions of our constructs accumulated in the tumor (Figure 2). The accumulation of nontargeting constructs in tumors has been demonstrated in multiple studies, including the similar accumulation of epidermal growth factor receptor (EGFR)–targeted and nontargeted liposomes in EGFR-expressing tumors [31] as well as HER2-targeted and nontargeted liposomes in HER2-expressing models [32]. This accumulation is hypothesized to be due to the enhanced permeability effect, caused by leaky tumor vasculature [33,34], and the absence of a functional lymphatic system, leading to retention of constructs [6,30].

The Role of Avidity and Internalization

While the relationship between affinity and target inhibition is well established, the relationship between valency on cell-based target binding and inhibition is less appreciated, although potentially more robust in the context of cell-based assays. This was shown in a recent study in which EGFR-binding Fab and IgG demonstrated log-fold or better binding and target inhibition with bivalency [35].

Increasing the cell binding functional affinity (avidity) of all our constructs using a homodimer peptide does not increase the quantitative tumor levels and limits tumor penetration (Figures 3*G* and 4). These findings correlate with the work on HER2 binding antibodies [25], where the investigators demonstrated a decrease in quantitative tumor levels and penetration with increasing affinity and internalization. The lower quantitative levels of the targeted *versus* nontargeting controls, as well as the monomeric *versus* homodimeric constructs, are likely due to internalization and degradation of the targeted constructs.

An increase in cell binding was not seen in the Fab construct going from a monomer peptide to a homodimer peptide (Figure 3*F*). Although not explored in this study, the space between two peptides on a linker may not provide sufficient benefit to translate into an increase in the cell binding affinity. Bivalent binding has, however, been shown to be important for internalization [36], and although an increase in cell binding affinity is not seen, in our *in vitro* internalization study, the monovalent Fab did not internalize, whereas the homodimer-conjugated Fab did (Figure 6*C*).

The internalization of the homodimer-conjugated Fab may also contribute to the decreased tumor penetration seen with the Fab homodimer peptide–conjugated construct (Figure 4*I*). Increasing the valency of the IgG and $F(ab)_2$ increased the total internalization at 10 nM for the IgG and significantly at 100 nM for the $F(ab)_2$. Increasing the valency particularly on our bivalent constructs may lead to cross-linking of more receptors and more robust internalization as has been demonstrated by glycosylphosphatidylinositol (GPI)-anchored folate receptors [37].

Contrary to predictions that increased affinity and decreased penetration seen in single dose studies may translate into poor efficacy, we demonstrate that increasing the avidity of our IgG translates into superior efficacy (Figure 5*A*). This is likely due to several factors such as more effective inhibition of proliferation and inhibition of the Erk1/2 signaling pathway that drives FGF19–FGFR4-mediated proliferation [38] (Figure 5, *B* and *C*). In addition, we demonstrate that one can dose through the "binding site barrier" (Figure 5*D*) [7].

Improved retention with increased avidity has been demonstrated using diabodies to investigate the role of valency on tumor uptake [13,17]. Although we do not see higher quantitative levels with increased valency (most likely due to internalization and consumption), our study demonstrates that increasing the valency can be an efficient way to increase the efficacy of targeting molecules.

In conclusion, the most promising candidate for FGFR4 antibody–targeted therapies would be the homodimer peptide–conjugated IgG. With an optimal PK profile and MW, this construct demonstrated effective inhibition of FGFR4-mediated proliferation pathways, which directly translated into superior efficacy. In general, increasing the valence of a receptor-targeted therapy is an effective way to increase efficacy.

Acknowledgments

We thank M. Ong for his technical expertise with conjugation, E. Corner and J. Hoye for help with scaffold generation, and J. Churchman for help running the Biacore experiment.

References

[1] Tunggal JK, Cowan DS, Shaikh H, and Tannock IF (1999). Penetration of anticancer drugs through solid tissue: a factor that limits the effectiveness of chemotherapy for solid tumors. *Clin Cancer Res* **5**, 1583–1586.

[2] Sedlacek HH, Seemann G, Hoffmann D, Czech J, Lorenz P, Kolar C, and Bosslet K (1992). Antibodies as carriers of cytotoxicity. In *Contributions to Oncology.* Vol 43. H Huber and W Queiber (Eds). Karger, Basel, Switzerland, pp. 74–75.

[3] Ackerman ME, Pawlowski D, and Wittrup KD (2008). Effect of antigen turnover rate and expression level on antibody penetration into tumor spheroids. *Mol Cancer Ther* **7**, 2233–2240.

[4] Chaplin DJ, Olive PL, and Durand RE (1987). Intermittent blood flow in a murine tumor: radiobiological effects. *Cancer Res* **47**, 597–601.

[5] Heldin CH, Rubin K, Pietras K, and Ostman A (2004). High interstitial fluid pressure—an obstacle in cancer therapy. *Nat Rev Cancer* **4**, 806–813.

[6] Jain RK (1994). Barriers to drug delivery in solid tumors. *Sci Am* **271**, 58–65.

[7] Saga T, Neumann RD, Heya T, Sato J, Kinuya S, Le N, Paik CH, and Weinstein JN (1995). Targeting cancer micrometastases with monoclonal antibodies: a binding-site barrier. *Proc Natl Acad Sci USA* **92**, 8999–9003.

[8] Fujimori K, Covell DG, Fletcher JE, and Weinstein JN (1989). Modeling analysis of the global and microscopic distribution of immunoglobulin G, F(ab′)2, and Fab in tumors. *Cancer Res* **49**, 5656–5663.

[9] Teillaud JL (2012). From whole monoclonal antibodies to single domain antibodies: think small. *Methods Mol Biol* **911**, 3–13.

[10] Kim SJ, Park Y, and Hong HJ (2005). Antibody engineering for the development of therapeutic antibodies. *Mol Cells* **20**, 17–29.

[11] Minchinton AI and Tannock IF (2006). Drug penetration in solid tumours. *Nat Rev Cancer* **6**, 583–592.

[12] Thurber GM, Zajic SC, and Wittrup KD (2007). Theoretic criteria for antibody penetration into solid tumors and micrometastases. *J Nucl Med* **48**, 995–999.

[13] Adams GP, Schier R, McCall AM, Crawford RS, Wolf EJ, Weiner LM, and Marks JD (1998). Prolonged *in vivo* tumour retention of a human diabody targeting the extracellular domain of human HER2/neu. *Br J Cancer* **77**, 1405–1412.

[14] Adams GP, Schier R, McCall AM, Simmons HH, Horak EM, Alpaugh RK, Marks JD, and Weiner LM (2001). High affinity restricts the localization and tumor penetration of single-chain fv antibody molecules. *Cancer Res* **61**, 4750–4755.

[15] Nelson AL (2010). Antibody fragments: hope and hype. *MAbs* **2**, 77–83.

[16] Yokota T, Milenic DE, Whitlow M, and Schlom J (1992). Rapid tumor penetration of a single-chain Fv and comparison with other immunoglobulin forms. *Cancer Res* **52**, 3402–3408.

[17] Nielsen UB, Adams GP, Weiner LM, and Marks JD (2000). Targeting of bivalent anti-ErbB2 diabody antibody fragments to tumor cells is independent of the intrinsic antibody affinity. *Cancer Res* **60**, 6434–6440.

[18] Zahnd C, Kawe M, Stumpp MT, de Pasquale C, Tamaskovic R, Nagy-Davidescu G, Dreier B, Schibli R, Binz HK, Waibel R, et al. (2010). Efficient tumor targeting with high-affinity designed ankyrin repeat proteins: effects of affinity and molecular size. *Cancer Res* **70**, 1595–1605.

[19] Adams GP, Tai MS, McCartney JE, Marks JD, Stafford WF III, Houston LL, Huston JS, and Weiner LM (2006). Avidity-mediated enhancement of *in vivo* tumor targeting by single-chain Fv dimers. *Clin Cancer Res* **12**, 1599–1605.

[20] Huang H, Lai JY, Do J, Liu D, Li L, Del Rosario J, Doppalapudi VR, Pirie-Shepherd S, Levin N, Bradshaw C, et al. (2011). Specifically targeting angiopoietin-2 inhibits angiogenesis, Tie2-expressing monocyte infiltration, and tumor growth. *Clin Cancer Res* **17**, 1001–1011.

[21] Blumenthal RD, Fand I, Sharkey RM, Boerman OC, Kashi R, and Goldenberg DM (1991). The effect of antibody protein dose on the uniformity of tumor distribution of radioantibodies: an autoradiographic study. *Cancer Immunol Immunother* **33**, 351–358.

[22] Rader C, Turner JM, Heine A, Shabat D, Sinha SC, Wilson IA, Lerner RA, and Barbas CF (2003). A humanized aldolase antibody for selective chemotherapy and adaptor immunotherapy. *J Mol Biol* **332**, 889–899.

[23] Doppalapudi VR, Huang J, Liu D, Jin P, Liu B, Li L, Desharnais J, Hagen C, Levin NJ, Shields MJ, et al. (2010). Chemical generation of bispecific antibodies. *Proc Natl Acad Sci USA* **107**, 22611–22616.

[24] Ho HK, Pok S, Streit S, Ruhe JE, Hart S, Lim KS, Loo HL, Aung MO, Lim SG, and Ullrich A (2009). Fibroblast growth factor receptor 4 regulates proliferation, anti-apoptosis and alpha-fetoprotein secretion during hepatocellular carcinoma progression and represents a potential target for therapeutic intervention. *J Hepatol* **50**, 118–127.

[25] Rudnick SI, Lou J, Shaller CC, Tang Y, Klein-Szanto AJ, Weiner LM, Marks JD, and Adams GP (2011). Influence of affinity and antigen internalization on the uptake and penetration of anti-HER2 antibodies in solid tumors. *Cancer Res* **71**, 2250–2259.

[26] Lin BC, Wang M, Blackmore C, and Desnoyers LR (2007). Liver-specific activities of FGF19 require Klotho beta. *J Biol Chem* **282**, 27277–27284.

[27] Yu SJ, Zheng L, Ladanyi M, Asa SL, and Ezzat S (2004). Sp1-mediated transcriptional control of fibroblast growth factor receptor 4 in sarcomas of skeletal muscle lineage. *Clin Cancer Res* **10**, 6750–6758.

[28] Fleuren ED, Versleijen-Jonkers YM, Heskamp S, Roeffen MH, Bouwman WH, Molkenboer-Kuenen JD, van Laarhoven HW, Oyen WJ, Boerman OC, and van der Graaf WT (2013). The strength of small: improved targeting of insulin-like growth factor-1 receptor (IGF-1R) with F(ab′)-R1507 fragments in Ewing sarcomas. *Eur J Cancer*, E-pub ahead of print.

[29] Sandström K, Haylock AK, Spiegelberg D, Qvarnström F, Wester K, and Nestor M (2012). A novel CD44v6 targeting antibody fragment with improved tumor-to-blood ratio. *Int J Oncol* **40**, 1525–1532.

[30] Wittrup KD, Thurber GM, Schmidt MM, and Rhoden JJ (2012). Practical theoretic guidance for the design of tumor-targeting agents. *Methods Enzymol* **503**, 255–268.

[31] Mamot C, Drummond DC, Noble CO, Kallab V, Guo Z, Hong K, Kirpotin DB, and Park JW (2005). Epidermal growth factor receptor–targeted immunoliposomes significantly enhance the efficacy of multiple anticancer drugs *in vivo*. *Cancer Res* **65**, 11631–11638.

[32] Kirpotin DB, Drummond DC, Shao Y, Shalaby MR, Hong K, Nielsen UB, Marks JD, Benz CC, and Park JW (2006). Antibody targeting of long-circulating lipidic nanoparticles does not increase tumor localization but does increase internalization in animal models. *Cancer Res* **66**, 6732–6740.

[33] Sands H, Jones PL, Shah SA, Palme D, Vessella RL, and Gallagher BM (1988). Correlation of vascular permeability and blood flow with monoclonal antibody uptake by human Clouser and renal cell xenografts. *Cancer Res* **48**, 188–193.

[34] Dvorak HF, Nagy JA, Dvorak JT, and Dvorak AM (1988). Identification and characterization of the blood vessels of solid tumors that are leaky to circulating macromolecules. *Am J Pathol* **133**, 95–109.

[35] Zhou Y, Goenaga AL, Harms BD, Zou H, Lou J, Conrad F, Adams GP, Schoeberl B, Nielsen UB, and Marks JD (2012). Impact of intrinsic affinity on functional binding and biological activity of EGFR antibodies. *Mol Cancer Ther* **11**, 1467–1476.

[36] Kyriakos RJ, Shih LB, Ong GL, Patel K, Goldenberg DM, and Mattes MJ (1992). The fate of antibodies bound to the surface of tumor cells *in vitro*. *Cancer Res* **52**, 835–842.

[37] Mayor S, Rothberg KG, and Maxfield FR (1994). Sequestration of GPI-anchored proteins in caveolae triggered by cross-linking. *Science* **264**, 1948–1951.

[38] Lin BC and Desnoyers LR (2012). FGF19 and cancer. *Adv Exp Med Biol* **728**, 183–194.